OPEN ACCESS

University of BRISTOL

Peer reviewed version

Link to published version (if available):
10.1021/acs.jpcb.6b02979

Link to publication record in Explore Bristol Research
PDF-document

University of Bristol - Explore Bristol Research

General rights

Distinguishing Population and Coherence Transfer Pathways in a Metal Dicarbonyl Complex using Pulse-Shaped 2DIR Spectroscopy

Hugo J.B. Marroux and Andrew J. Orr-Ewing*

School of Chemistry, University of Bristol, Bristol BS8 1TS, UK

* Author for correspondence: a.orr-ewing@bristol.ac.uk; +44 117 9287672

Abstract: Collection of two dimensional infrared (2DIR) spectra using two ultrafast, broadband infrared pump pulses followed by an ultrafast probe pulse optimizes the experimental time and frequency resolution, but can also introduce quantum beat and coherence transfer pathways. The associated coherent dynamics create intensity oscillations and add extra features to 2DIR spectra. We describe a method to suppress these pathways using pump-pulse shaping, without significantly degrading the time and spectral resolution. We illustrate the method for a rhodium dicarbonyl complex, acetylacetonato dicarbonyl rhodium, to establish the relative importance of coherence and population transfer between carbonyl symmetric and asymmetric stretching modes. Our technique effectively suppresses the quantum beats. Comparison of peak intensities obtained with shaped and unshaped pump pulses demonstrates that coherence transfer does not play a significant role in the 2DIR spectrum of RDC in this spectral region.

Introduction

The development and use of multidimensional spectroscopy over frequencies spanning the terahertz to ultraviolet regions has enabled important advances in physical chemistry during the past decade.[1] These methods draw inspiration from techniques originally introduced for 2D NMR spectroscopy,[2] but can probe molecular dynamics on much shorter timescales. The first multidimensional experiment at optical wavelengths was conducted in the IR; a spectrum was

collected in the frequency domain, using a pump/probe technique in which the central frequency of a narrowband IR pump pulse was scanned through resonance with the amide I stretching mode of N-methylacetamide.[3] The two dimensional infrared (2DIR) spectrum was obtained by monitoring the resulting changes in intensity in the probe pulse spectrum. This technique is referred to as double-resonance 2DIR (DR-2DIR)[4] because the two pump interactions in the 3rd order molecular response are simultaneous and degenerate. The DR-2DIR method provides valuable dynamical insights, but it does not offer optimal time resolution because the bandwidth of the pump pulse must be smaller than the homogenous linewidth of the molecular transition. Improvements were realized by implementing Fourier-Transform 2DIR (FT-2DIR),[5] which is analogous to modern methods of 2D-NMR. In FT-2DIR, the narrow-bandwidth pump pulse is replaced by two ultrafast broadband pulses separated by a time delay t_1 (the coherence time); these pulses provide the two pump interactions of the 3rd order molecular response, while retaining high time resolution. The Free Induction Decay (FID) of the coherence created by the first interaction is observed by projection into a population state by the second interaction after time t_1. Fourier transformation over t_1 retrieves the pump spectrum axis. The FID oscillates at the transition frequency and its decay rate contains information on the bandshape. Therefore, no spectral information is lost, and the broadband pulses provide optimal time resolution. Comparison of DR-2DIR and FT-2DIR experiments by Hamm and coworkers showed the improvement of resolution achieved with the latter method,[4] but also revealed two different artefacts induced by the broadband pump pulses.

In FT-2DIR, because each pump pulse is broadband, the two pump interactions do not have to be degenerate and will introduce new interaction pathways that are inaccessible in DR-2DIR.

Those new pathways can generate quantum beats (QB) and coherence transfer (CT) that might mask population kinetics and produce unwanted features in the spectrum. QBs arise from the coherent super-position of excited states, and in 2D electronic spectroscopy they revealed excitonic couplings in light harvesting complexes.[6,7] However, in 2DIR where the majority of experiments focus on population states to extract structural or dynamical information, it is often desirable to eliminate QB oscillations. CT occurs when a coherent superposition of two states, $|a\rangle\langle b|$ is transferred to another coherent superposition of states $|a\rangle\langle c|$. CT has been studied to understand lineshapes of exchanging species in 1D[8] and 2D IR spectra,[9] and has also been invoked to account for additional features seen exclusively in FT-2DIR.[10] In an early study of acetylacetonato dicarbonyl rhodium (RDC), Khalil *et al.*[11] reported both CT features and QB signatures in their spectra. Wright and coworkers[12,13,14] also identified CT pathways in the same system using a different phase matching geometry. A recent simulation by Baiz *et al.* contrasts with these earlier RDC studies because it argued that CT made negligible contributions to the FT-2DIR spectrum of another metal carbonyl, Mn_2CO_{10}.[15] Here, we address the direct experimental determination of the significance of CT and QB pathways relative to conventional population transfer (PT) between states, and introduce a method to quantify the extent to which they impact on FT-2DIR spectra.

We have undertaken a new study of the RDC system in which a pulse shaping method allows active selection of population and population-transfer Feynman pathways, while suppressing QB and CT effects. Direct amplitude comparison with conventional FT-2DIR data quantifies the relative contributions of these various processes. We also present spectral simulations to identify an upper limit to the CT rate, and by comparing this rate to the dephasing

time of our system, we conclude that CT does not occur to any significant extent in RDC and hence has negligible impact in the FT-2DIR spectrum.

Experimental section

We use a mid-IR pulse-shaping method developed by Zanni and coworkers[16] to collect our spectra. Full details of our laser system have been presented elsewhere.[17] In brief, we use a wedged CaF_2 beam splitter to divide the 5000 nm mid-IR output of a Coherent Inc. optical parametric amplifier (OPerA Solo), equipped with a difference frequency generation crystal, to prepare pump (4.5 μJ) and probe (250 nJ) pulses. We use an acousto-optic modulator (AOM) based pulse shaper (Quickshape, PhaseTech Spectroscopy Inc.) to convert the single pump pulse into two pump pulses with programmable time delay and relative phase. The pump pulse energy is 800 nJ at the sample. The original arbitrary waveform generator (AWG) for the PhaseTech pulse shaper was replaced by a PXDAC4800D AWG from Systemware Europe Ltd, chosen because its higher sampling rate (300MHz) enhances the pulse shaping. Pump pulses and the probe pulse are focused into our sample to respective spot sizes of 150 μm and 100 μm, and all the pulse polarizations are horizontal. The sample sits in a Harrick cell between two 1.5 mm thick CaF_2 windows separated by a 100-μm Teflon spacer. The transmitted probe beam is sent to a Horiba spectrometer (150 lines per mm grating, blazed for 5000 nm) and imaged onto a 128-element Mercury-Cadmium-Telluride array (Infrared Systems Development Corp.). We scan the coherence time delay with the pulse shaper in 80 fs time steps up to 7500 fs to sample the entire FID. We program the AOM to shift our observations into a rotating frame of 1950 cm^{-1} to reduce the observed frequency of the coherences and hence reduce the number of time points to collect. To eliminate the scatter from pump pulses and contributions from transient absorption signals, we use a 2-by-2 phase cycling

scheme.[18] The time domain data are baseline corrected with a linear fit function, windowed with a Gaussian function with adjustable width, zero-padded 8 times and Fourier transformed to obtain our 2D spectra. Varying the pump-probe time delay (t_2) scans the system dynamics up to 130 ps. Acetylacetonato dicarbonyl rhodium (RDC, 98%) and the solvent n-hexane were purchased from Sigma-Aldrich and used without further purification. Solutions were prepared to give an optical density of ≤0.6 on the carbonyl absorption bands of RDC.

Results and Discussion

RDC displays two resolved IR bands in the carbonyl stretch region, as shown in **Figure 1a.** The transitions at 2015 cm^{-1} and 2084 cm^{-1} are respectively assigned to the carbonyl asymmetric (A) and symmetric (S) stretches. **Figure 1b** shows the different vibrational states considered in our analysis. To evaluate the contributions of QB and CT in our spectrum, we first collected FT-2DIR data using the broadband pump pulse spectrum reported as a dashed line in **Figure 1a** to compare to the 2DIR spectra observed in previous studies.[4,11] The resulting 2DIR spectrum is shown in **Figure 1c** for a waiting time t_2 = 8.6 ps after the second of the pump pulses, and **Figure 1d** shows the intensity variations of selected features with increasing pump-probe time delay.
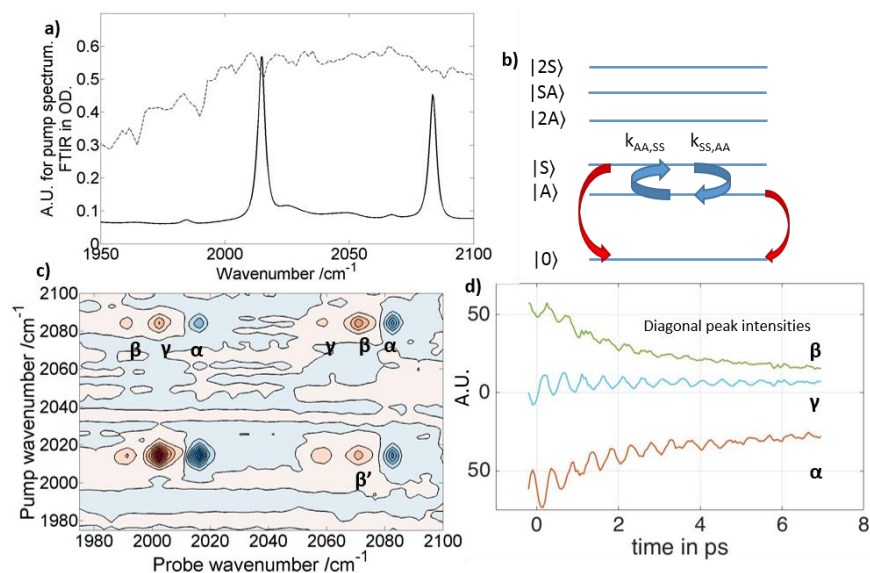
Fig. 1: Spectra and kinetics for RDC in n-hexane. **a)** FTIR (solid line) and scaled pump pulse (dotted line) spectra. **b)** Energy diagram of the system eigenstates, with blue arrows indicating population transfer between excited symmetric $|S\rangle$ and asymmetric $|A\rangle$ stretching states and red arrows denoting vibrational decay. **c)** 2DIR spectrum of RDC with the full-pump pulse, obtained at $t_2 = 8.6$ ps. **d)** Kinetic traces of diagonal peaks at pump wavenumbers around 2084 cm^{-1}.

A large number of Feynman pathways can contribute to the spectral features, and the Supporting Information presents the associated diagrams and connects them to their corresponding spectral features. Here, we describe the main contributions for each of the observed peaks, and focus on the row in the 2DIR spectrum corresponding to pumping the symmetric stretching vibration around 2084 cm^{-1}. Peak labels introduced below are the same for the corresponding peaks in the part of the spectrum resulting from pumping the asymmetric stretch near 2015 cm^{-1}.

The negative-going bleaches contain contributions from excited state stimulated emission and ground state absorption (e.g., peaks labelled **α**). The excited state absorptions (positive peaks labelled **β**) are shifted from the corresponding bleaches by -12 cm^{-1} and -24 cm^{-1} for the diagonal and off-diagonal features respectively. These contributions derive from conventional pathways

common to many 2DIR experiments. The other pathways incorporate CT or PT steps and QB effects. Peak γ has potential contributions from both CT and PT mechanisms. The CT contribution to the γ peak is summarized by Feynman diagram 1 in **Figure 2** in which the third interaction prepares a coherence involving a two-quanta excited state, and the overall diagram involves two CT steps. Tokmakoff and co-workers invoked double-CT pathways of this type to explain their observations for RDC. Double-CT also contributes to bleach features, as illustrated by diagram 2 in **Figure 2**. Single CT pathways are not shown because they are expected to be weak, according to polarization arguments presented by Zanni[19] and Tokmakoff;[11] however, they were observed by Wright and co-workers in RDC.[12-14] We compare the significance of the two types of CT mechanism later in the context of our data.
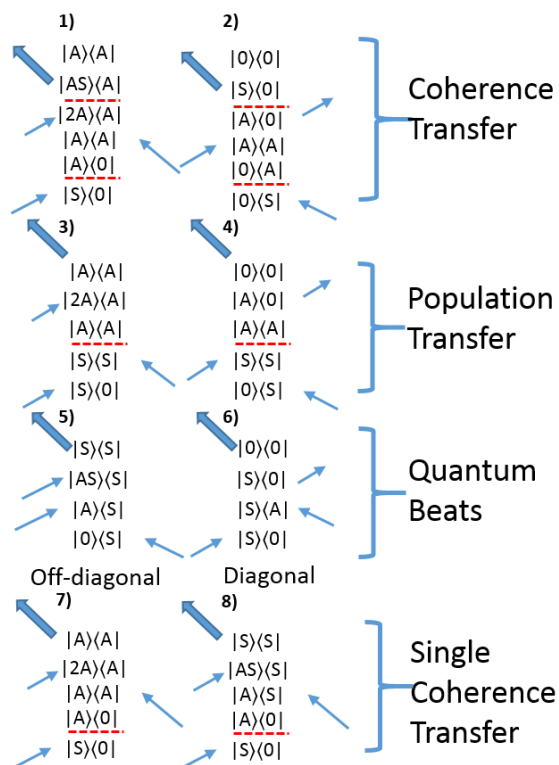

Fig. 2: Example Feynman pathways for the various dynamical processes discussed in the text. Red dashed lines indicate population or coherence transfer steps.

Figure 2 includes examples of Feynman diagrams incorporating population transfer (diagrams 3 and 4). As is explained in the Supporting Information, these PT mechanisms will contribute to the peaks labelled **γ** and to the off-diagonal bleach labelled **α**, but PT also affects all the spectral features by de-populating conventional pathways. **Figure 1d** shows the time dependence of the diagonal peaks labelled **α**, **β** and **γ** obtained by varying the pump-probe time delay t_2 (between the second and third interactions). Oscillations caused by QBs (or *interstate coherences*) are evident in all the kinetic traces. Diagrams 5 and 6 in **Figure 2** account for these oscillations because after the second interaction the system is in a coherent superposition $|A\rangle\langle S|$. Non-oscillatory peak intensity changes are the result of PT; for example, the time constant for vibrational decay of the metal carbonyl is approximately 50 ps.[10] The Supporting Information includes Feynman diagrams for all the pathways yielding QBs, and QB features are centered on 8 of the 12 peaks present in our spectrum. However, beating more subtly affects the entire spectrum because the lineshapes of those transitions are much broader than the absorptive lineshapes. Indeed, in QB pathways, rephasing and non-rephasing diagrams are not at the same frequency, preventing phase twist cancellation. **Figure S2** shows the isolated lineshapes for the QB pathways at two different waiting times, calculated using dynamical response functions similar to those used by Hamm and Zanni.[20] Accurate analysis of the time-dependent intensities of the type shown in **Figure 1d** requires simulation of the dynamics using a kinetic model. In addition to PT rates, the model must also incorporate the QB oscillations and dephasing for each energy spacing between bright states spanned by the pump pulse spectrum. This complexity can greatly increase the number of parameters describing the observations and adversely affect the accuracy of fits to obtain their values.

In our pulse-shaping experiments, we instead suppress the QB oscillations and limit the accessible pathways to just conventional and PT pathways. Fayer and coworkers used a similar approach to reduce QB oscillations in their analysis of center line slope changes in 2DIR spectra of a metal-organic framework.[21] We control the contributions to our spectra by shaping the spectrum of the pump pulses so that only one transition can be resonant with our excitation. The interactions leading to QB and double-CT always have their first and second interactions with different transitions, but this type of interaction cannot occur in our pulse-shaped experiment. **Figure 3a** shows the pump spectrum for each of these two half-pump experiments (solid blue and red lines), each covering a single transition, as well as the full-pump spectrum covering the two transitions (dashed line). The 2DIR spectra collected for the two half-pump schemes are shown in **Figure 3b** and **3c**, and contain a subset of the peaks in the full-pump spectrum in **Figure 1c**. In a regular 2DIR data acquisition procedure using an AOM pulse shaper, each laser shot corresponds to a different time delay and pump-pump relative phase. To compare the amplitudes between the three types of pump spectrum needed for our analysis, we introduce the three pump spectra on consecutive shots for a fixed time delay and relative phase. In this data collection scheme, all the data sets are for the same experimental conditions (e.g., pulse overlap and time delay), and we can average over power fluctuations. We choose not to compress our pulses, so that when we reduce our bandwidth by half, the pulse duration does not significantly change as shown by the cross-correlation with the probe pulse taken in Germanium (**Figure S7**).
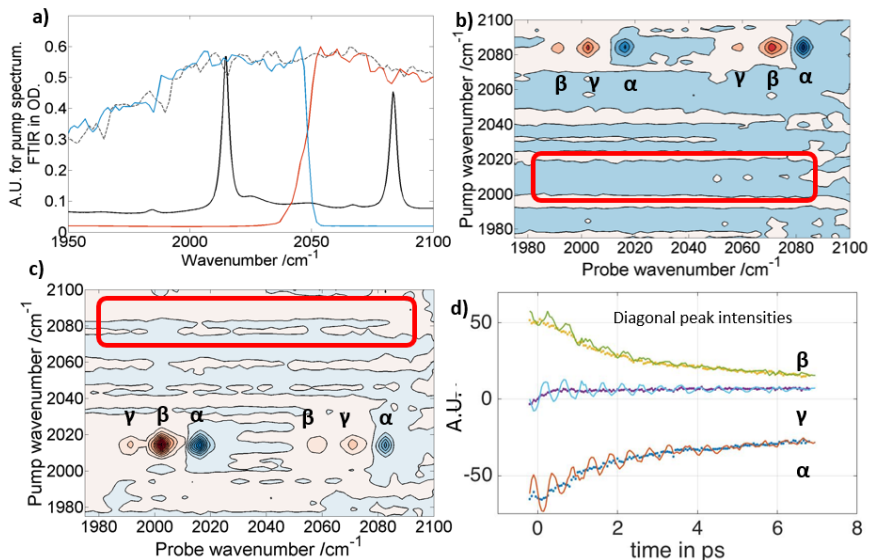
Fig. 3: a) RDC FTIR spectrum (solid black line), and scaled spectra of the full-pump pulse (dotted line), and the two half-pump pulses (red and blue solid lines). **b)** half-pump 2DIR spectrum of RDC pumped with the red spectrum in **a)**. **c)** half-pump 2DIR spectrum of RDC pumped with the blue spectrum in **a)**. **d)** Kinetic traces of the diagonal peaks centered at 2084 cm^{-1} in the full-pump (solid lines) and half-pump (dots) experiments.

We observe peak γ in all three spectra, confirming that PT, and not exclusively CT, must be contributing. To assess the effect of CT on the spectra, we first consider the possibility of single-CT pathways. In our half-pump experiments, single-step CT might still contribute, and will create features in the un-pumped part of the spectrum because diagrams like number 8 in **Figure 2** introduce coherent oscillations during t_1 at both $\omega_{S,0}$ and $\omega_{A,0}$ fundamental frequencies. We inspected our data in the un-pumped parts of our spectra (outlined by the red boxes in **Figure 3b** and **c**) and for different waiting times and did not observe any features, so we can discount significant single-step CT. This deduction confirms observations by Tokmakoff[11] and Zanni.[19] The absence of single-CT signatures is a first hint of whether CT will influence our FT-2DIR spectra.

Before we investigate double-CT, we need to characterize PT effects in the half-pump spectra in **Figures 3b** and **c**. **Figure 3d** compares the integrated peak time-evolutions for the

diagonal peaks **α**, **β** and **γ** excited in the region of the 2084 cm^{-1} symmetric stretch band when the half-pump (dots) or full-pump (solid lines) bandwidth is used. Quenching of the oscillations in the half-pump kinetic traces proves the capability of our technique to suppress selectively the QB pathways. The dynamics seen in the time-dependent changes to half-pump peak intensities are mainly due to PT. **Figure S8** shows the kinetics of all the γ peaks for the half-pump and full-pump experiments.

Solving the coupled differential equations for the transfer of population between carbonyl symmetric and asymmetric stretching modes (see Eq. S1 of Supporting Information) shows that population exchange occurs with single exponential kinetics and a rate coefficient $k_{obs} = k_{S,S \to A,A} + k_{A,A \to S,S}$ (with A,A and S,S denoting population states). The overall population of these states also undergoes exponential decay through vibrational relaxation, and we include this in our fit function. To follow the population of $|S\rangle\langle S|$ transferring to $|A\rangle\langle A|$, we monitor the intensity of diagonal and off-diagonal peaks γ at the pump frequency $\omega_{S,0}$, and to monitor the population of $|A\rangle\langle A|$ transferred to $|S\rangle\langle S|$ we analyse the corresponding peak γ at pump frequency $\omega_{A,0}$. For the simulation of the half-pump spectrum, these peak amplitudes depend only on the transfer rate coefficients $k_{S,S \to A,A}$ and $k_{A,A \to S,S}$ respectively (see **Figure S3**).

The four peak-γ traces were simultaneously fitted to a sum of an exponential growth with $k_{obs} = (3.23 \pm 0.05 \text{ps})^{-1}$ and an exponential decay with $k_{\text{vib decay}} = (53.3 \pm 0.5 \text{ ps})^{-1}$. With the harmonic relation for the transition dipole moments, $\mu_{2A,A} = \sqrt{2}\,\mu_{A,0}$ the ratio of the off-diagonal γ-peak intensities at equilibrium simply becomes the ratio of the equilibrium rate coefficients (see the SI for a derivation). We averaged the peak intensities for t_2 between 13 and 14 ps to minimize the

effect of vibrational decay, and obtain $\frac{I_{\omega_A}^{\gamma}}{I_{\omega_S}^{\gamma}} = \frac{15.6}{20.0} = \frac{k_{A,A\rightarrow S,S}}{k_{S,S\rightarrow A,A}}$. Here, $I_{\omega_A}^{\gamma}$ is the intensity of the off-diagonal peak γ at the pump frequency $\omega_A = 2014$ cm^{-1} and at equilibrium, and similarly for $I_{\omega_S}^{\gamma}$.

Combining this result with $k_{obs} = k_{S,S\rightarrow A,A} + k_{A,A\rightarrow S,S}$ we get $k_{S,S\rightarrow A,A} = (5.7 \pm 0.1)^{-1} \, ps^{-1}$ and $k_{A,A\rightarrow S,S} = (7.3 \pm 0.12)^{-1} \, ps^{-1}$. The ratio of the rate coefficients is in agreement with expectations from detailed balance.

To isolate the oscillatory part of the traces, we subtracted kinetic traces derived from the half-pump experiments from those for the full-pump for specific spectral features, and Fourier transformed the remaining QB oscillations. The full FIDs can instead be fitted to an oscillatory function superimposed on a decay function, but our method clearly isolates the QB signatures prior to fitting. A resulting peak at 69 cm^{-1} matches the frequency difference between the two modes, and the linewidth of this peak matches the linewidths of the fundamental transitions for the symmetric and asymmetric stretches (see **Figure S7**) indicating that both excited states are subject to the same bath fluctuations.

To determine the influence of double-CT in our spectra, we now compare the kinetic traces after the dephasing of the quantum beats. The dephasing does not affect CT pathways because they lead to population states during the waiting time. In the case of a full-pump spectrum, at waiting times larger than 6 ps, the only pathways contributing to the peaks are PT, double-CT and the conventional pathways. In the case of the half-pump experiment, only the conventional and PT pathways contribute. By comparing the intensity difference between the two experiments, we determine the contribution from double-CT. At $t_2 > 6$ ps, all the traces have the same intensities, which shows that CT only has a small influence on our spectral features.

We make a quantitative estimate of the importance of double-CT pathways by simulating our spectra using response functions in which we explicitly include each Feynman pathway of the system in the full-pump and half-pump cases. To compute the PT effect on all the pathways, we adapt the method of Hochstrasser and coworkers.[22, 23, 24] To model CT, we solve the system of differential equation in Eq. S6 using an approach similar to these authors,[9] but extended to include excited state transfer. The double-CT contributions considered here are governed by the rate coefficients $k_{A,0 \to S,0}$, $k_{2A,A \to AS,A}$, $k_{AS,S \to AS,A}$ and $k_{2S,S \to AS,S}$ and the rate coefficients for the reverse processes. Coherence transfer steps like $|2A\rangle\langle A| \to |2A\rangle\langle S|$ are not incorporated because field emission from this type of coherence to a population state is not allowed. To monitor the extent of CT, we compute the intensity of the 2084 cm^{-1} diagonal bleach peak with only PT and conventional pathways (analogous to the half pump experiment) and for all pathways (analogous to the full-pump experiment). We choose to monitor the bleach because its intensity dependence on CT is determined by only one rate coefficient $k_{S,0 \to A,0}$ (assuming that the reverse rate coefficient is approximately the same). **Figure 4a** shows the simulated intensity of the bleach in both cases for a CT rate coefficient of (380 fs)$^{-1}$ previously reported in ref.11. In both traces, we observe the expected behavior for all the mechanisms considered: a few picoseconds bleach recovery due to PT in both types of measurement, and oscillations and an offset caused by QB and CT respectively in the full-pump case. With our experimental signal-to-noise ratios, we can distinguish intensity differences down to 7% of the full-pump trace intensity. To bring the two traces to within 7% of one another, we need to decrease the CT rate to (250 ps)$^{-1}$ as illustrated in **Figure 4b**. This rate is much slower than the system lifetime, so we conclude that CT does not play a significant role in

the spectrum observed by conventional FT-2DIR, and that all the observed spectral features and their dynamics are due to PT, QB and conventional 2DIR Feynman pathways.
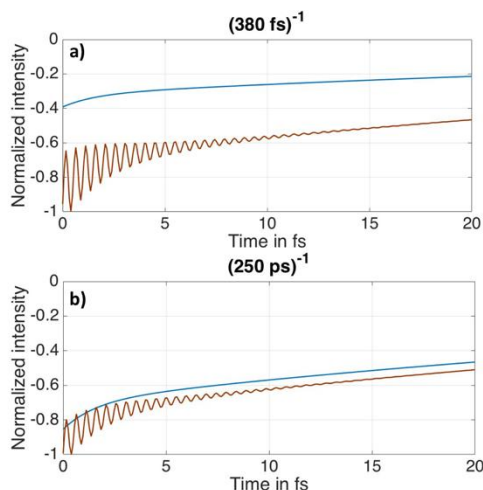
Fig. 4: Kinetic traces obtained from spectral simulations described in the text for CT rate coefficients of: **a)** $(380 \text{ fs})^{-1}$; **b)** $(250 \text{ ps})^{-1}$.

Conclusions

We have demonstrated an experimental method based on IR pulse shaping that directly identifies contributions to a 2DIR spectrum of two coupled oscillators from population and coherence transfer pathways. The method is illustrated in a study of the acetylacetonato dicarbonyl rhodium complex in n-hexane. This rhodium dicarbonyl complex was selected as a model system because it was previously argued to show significant coherence transfer between vibrationally excited levels of the symmetric and asymmetric stretching modes, which lie close in energy. Suppression of the coherence transfer pathways by IR pulse shaping demonstrates that population transfer dominates the exchange between these two modes, and that coherence transfer is too slow to be important.

Supporting Information Available: All Feynman pathways contributing to all features observed in the 2DIR spectra; Summaries of the kinetic models used to analyse population and coherence transfer; Derivations of relationships used in the analysis. This information is available free of charge via the Internet at http://pubs.acs.org

All experimenal data are archived in the University of Bristol's Research Data Storage Facility and are accessible using the DOI: 10.5523/bris.bx321kl8aur51legup83jb9hw.

References

1. Elsaesser, T.; Reimann, K.; Woerner, M. Focus: Phase-Resolved Nonlinear Terahertz Spectroscopy-from Charge Dynamics in Solids to Molecular Excitations in Liquids. *J. Chem. Phys.* **2015,** *142*, 212301.
2. Jeener, J.; Meier, B. H.; Bachmann, P.; Ernst, R. R. Investigation of Exchange Processes by 2-Dimensional NMR-Spectroscopy. *J. Chem. Phys.* **1979,** *71*, 4546-4553.
3. Hamm, P.; Lim, M. H.; Hochstrasser, R. M. Structure of the Amide I Band of Peptides Measured by Femtosecond Nonlinear-Infrared Spectroscopy. *J. Phys. Chem. B* **1998,** *102*, 6123-6138.
4. Cervetto, V.; Helbing, J.; Bredenbeck, J.; Hamm, P. Double-Resonance Versus Pulsed Fourier Transform Two-Dimensional Infrared Spectroscopy: An Experimental and Theoretical Comparison. *J. Chem. Phys.* **2004,** *121*, 5935-5942.
5. Asplund, M. C.; Zanni, M. T.; Hochstrasser, R. M. Two-Dimensional Infrared Spectroscopy of Peptides by Phase-Controlled Femtosecond Vibrational Photon Echoes. *P. Natl. Acad. Sci. USA* **2000,** *97*, 8219-8224.
6. De Re, E.; Schlau-Cohen, G. S.; Leverenz, R. L.; Huxter, V. M.; Oliver, T. A. A.; Mathies, R. A.; Fleming, G. R. Insights into the Structural Changes Occurring Upon Photoconversion in the Orange Carotenoid Protein from Broadband Two-Dimensional Electronic Spectroscopy. *J. Phys. Chem. B* **2014,** *118*, 5382-5389.

7. Rafiq, S.; Dean, J. C.; Scholes, G. D. Observing Vibrational Wavepackets During an Ultrafast Electron Transfer Reaction. *J. Phys. Chem. A* **2015,** *119*, 11837-11846.

8. Wood, K. A.; Strauss, H. L. Broadening and Shifts of Vibrational Bands Due to the Effect of Thermal Chemical-Reactions. *J. Phys. Chem.* **1990,** *94*, 5677-5684.

9. Kim, Y. S.; Hochstrasser, R. M. Comparison of Linear and 2D IR Spectra in the Presence of Fast Exchange. *J. Phys. Chem. B* **2006,** *110*, 8531-8534.

10. Nee, M. J.; Baiz, C. R.; Anna, J. M.; McCanne, R.; Kubarych, K. J. Multilevel Vibrational Coherence Transfer and Wavepacket Dynamics Probed with Multidimensional IR Spectroscopy. *J. Chem. Phys.* **2008,** *129*.

11. Khalil, M.; Demirdoven, N.; Tokmakoff, A. Vibrational Coherence Transfer Characterized with Fourier-Transform 2D IR Spectroscopy. *J. Chem. Phys.* **2004,** *121*, 362-373.

12. Rickard, M. A.; Pakoulev, A. V.; Kornau, K.; Mathew, N. A.; Wright, J. C. Interferometric Coherence Transfer Modulations in Triply Vibrationally Enhanced Four-Wave Mixing. *J. Phys. Chem. A* **2006,** *110*, 11384-11387.

13. Rickard, M. A.; Mathew, N. A.; Pakoulev, A. V.; Kornau, K. M.; Wright, J. C. Frequency- and Time-Resolved Coherence Transfer Spectroscopy. *Abstr. Pap. Am. Chem. S.* **2007,** *233*, 515-PHYS.

14. Pakoulev, A. V.; Rickard, M. A.; Mathew, N. A.; Kornau, K. M.; Wright, J. C. Frequency-Domain Time-Resolved Four Wave Mixing Spectroscopy of Vibrational Coherence Transfer with Single-Color Excitation. *J. Phys. Chem. A* **2008,** *112*, 6320-6329.

15. Baiz, C. R.; Kubarych, K. J.; Geva, E. Molecular Theory and Simulation of Coherence Transfer in Metal Carbonyls and Its Signature on Multidimensional Infrared Spectra. *J. Phys. Chem. B* **2011,** *115*, 5322-5339.

16. Middleton, C. T.; Woys, A. M.; Mukherjee, S. S.; Zanni, M. T. Residue-Specific Structural Kinetics of Proteins through the Union of Isotope Labeling, Mid-IR Pulse Shaping, and Coherent 2D IR Spectroscopy. *Methods* **2010,** *52*, 12-22.

17. Roberts, G. M.; Marroux, H. J. B.; Grubb, M. P.; Ashfold, M. N. R.; Orr-Ewing, A. J. On the Participation of Photoinduced N-H Bond Fission in Aqueous Adenine at 266 and 220 nm: A Combined Ultrafast Transient Electronic and Vibrational Absorption Spectroscopy Study. *J. Phys. Chem. A* **2014,** *118*, 11211-11225.

18. Shim, S. H.; Zanni, M. T. How to Turn Your Pump-Probe Instrument into a Multidimensional Spectrometer: 2D IR and Vis Spectroscopies Via Pulse Shaping. *Phys. Chem. Chem. Phys.* **2009,** *11*, 748-761.

19. Ding, F.; Fulmer, E. C.; Zanni, M. T. Heterodyned Fifth-Order Two-Dimensional IR Spectroscopy: Third-Quantum States and Polarization Selectivity. *J. Chem. Phys.* **2005,** *123*, 094502.

20. Hamm, P.; Zanni, M. *Concepts and Methods of 2D Infrared Spectroscopy*. Cambridge University Press: 2011.

21. Nishida, J.; Tamimi, A.; Fei, H. H.; Pullen, S.; Ott, S.; Cohen, S. M.; Fayer, M. D. Structural Dynamics inside a Functionalized Metal-Organic Framework Probed by Ultrafast 2D IR Spectroscopy. *P. Natl. Acad. Sci. USA* **2014,** *111*, 18442-18447.

22. Kim, Y. S.; Hochstrasser, R. M. Chemical Exchange 2D IR of Hydrogen-Bond Making and Breaking. *P. Natl. Acad. Sci. USA* **2005,** *102*, 11185-11190.

23. Ha, J. H.; Kim, Y. S.; Hochstrasser, R. M. Vibrational Dynamics of N-H, C-D, and C=O Modes in Formamide. *J. Chem. Phys.* **2006,** *124*, 064508.

24. Park, J.; Ha, J. H.; Hochstrasser, R. M. Multidimensional Infrared Spectroscopy of the N-H Bond Motions in Formamide. *J. Chem. Phys.* **2004,** *121*, 7281-7292.

$|S\rangle$

$|A\rangle$